# EVOLUTION OF A COUNTER-ROTATING VORTEX PAIR IN A STABLY STRATIFIED FLUID

**Keiko K. Nomura†, Hideaki Tsutsui, Daniel Mahoney, Julie Crockett, James W. Rottman**
Department of Mechanical and Aerospace Engineering,
University of California, San Diego
La Jolla, CA 92093-0411, U.S.A.
†knomura@ucsd.edu

## ABSTRACT

The evolution of a counter-rotating vortex pair in a stably stratified fluid is investigated using direct numerical simulations. The study focuses on the short-wavelength instability occurring in this flow and subsequent decay of the vortices. With stable stratification, the instability exhibits an earlier onset and higher growth rate than in an unstratified flow. This is due to the enhanced strain that occurs when the vortices move closer together as a result of the generated baroclinic torque. The decay of the vortex pair is enhanced with stratification due to additional mechanisms present in the flow. Secondary vertical vortex structures form between the primary vortices which enables exchange of fluid in the transverse direction. Detrainment of fluid from the primary vortices by the generated baroclinic torque also contributes to the breakdown of the flow. Computed energy spectra show the evolution of the primary instability, development of harmonics, and late time behavior.

## INTRODUCTION

A counter-rotating vortex pair is a model flow of both practical and fundamental significance. Such a flow may be observed in the wake of an aircraft or at the small scales in sheared turbulence. In either case, it is of interest to understand the behavior of the flow in a density stratified environment. A counter-rotating vortex pair is known to exhibit a long-wavelength (Crow) instability (Crow, 1970) which results in a symmetric sinusoidal deformation of the vortex cores with wavelength of $8.6b_o$, where $b_o$ is the initial vortex spacing. The effect of ambient stratification on the Crow instability has been investigated by Garten et al. (2001). In unstratified fluids, laboratory experiments (Sarpkaya and Suthon, 1991, Thomas and Auerbach, 1994, Leweke and Williamson, 1998) and numerical simulations (Laporte and Corjon, 2000) have shown that a short-wavelength instability may also develop in a counter-rotating vortex pair. The short wave (elliptic) instability is associated with the ellipticity of the streamlines in the vortex cores due to the strain induced by one vortex on the other (Leweke and Williamson, 1998). The vortices exhibit an antisymmetric sinusoidal deformation with wavelength of order $b_o$. Recently, an experimental and numerical study by Delisi and Robbins (2000) showed the development of a short wave instability in stably stratified flows. The wavelength of the instability was found to be longer (approximately $b_o - 2b_o$) than that reported for unstratified flows. Their results indicate that stable stratification results in an earlier onset and a more rapid growth of the instability at the expense of the Crow instability. Results from large eddy simulations (LES) of vortex pairs in stably stratified fluid (Switzer and Proctor, 2000) indicate that the level of ambient stratification and turbulence determine whether the long-wave or short-wave instability dominates. Holzäpfel et al. (2001) also performed LES and showed that in the case of a quiescent atmosphere and ambient stratification, the decay of the vortices is controlled by the interaction of the short-wave instability and baroclinic vorticity. All three studies indicate that the short wave instability is enhanced with stable stratification. However, quantitative assessment of the instability and details of the associated physical processes are limited.

The objective of the present study is to further investigate the effects of stratification on the short-wavelength instability and subsequent nonlinear evolution of the flow. A more quantitative assessment of the instability is carried out. Growth rates of the instability are evaluated for a range of stratification levels. Energy spectra are computed and show the evolution of the primary instability, development of harmonics, and late time behavior. Detailed analysis is carried out to understand the development of structural features and the associated physical processes leading to the decay of the vortex pair.

## DIRECT NUMERICAL SIMULATIONS

The simulations are performed using a direct numerical simulation (DNS) code originally developed for stratified homogeneous turbulence (Gerz et al., 1989). The code solves the three-dimensional Navier-Stokes equations with the Boussinesq approximation. Figure 1 shows the coordinate axes and initial flow conditions. The simulations are initialized with a two-dimensional distribution of axial vorticity $\omega_y$ corresponding to a counter-rotating vortex pair and a three-dimensional random velocity perturbation. Uniform stable stratification ($d\rho/dz < 0$) is superimposed. The initial separation of the vortices is $b_o$. The dimensions of the computational domain are $L_x = 6b_o$, $L_y = 6b_o$, $L_z = 18b_o$, with resolution of 192 x 192 x 576 grid points, respectively. Periodic boundary conditions are employed in all three directions. The axial length, $L_y = 6b_o$, is short enough to effectively exclude the Crow instability while the transverse length, $L_x = 6b_o$, is long enough to minimize the effects of neighboring vortices. The vertical length, $L_z = 18b_o$, is extended to accommodate the downward descent of the vortices which leaves behind a wake. The Reynolds number of the vortex pair based on the initial circulation $\Gamma_o$ is $Re_\Gamma = \Gamma_o/\nu = 2400$. The Froude numbers, $Fr = W_o/Nb_o$, considered are $Fr = 2, 5, \infty$. Here, $W_o = \Gamma_o/2\pi b_o$ is the initial advection velocity of the vortices and $N$ is the buoyancy frequency ($N^2 = -(g/\rho_o)d\rho/dz$). The flow conditions considered represent relatively weak stratification ($Fr > 1$). Flows with strong stratifcation ($Fr \leq 1$) exhibit quite dif-

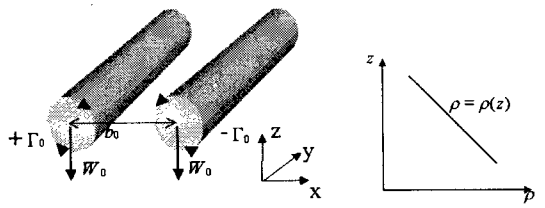


Figure 1: Coordinate system and initial conditions; counter-rotationg vortex pair and uniform stable stratification.

ferent behavior and are a subject of another study. Nondimensional time is $t^* = tW_o/b_o$.

## RESULTS

Figure 3 shows the evolution of the average axial and transverse vorticity magnitudes, $\Gamma_y$ and $\Gamma_x$, respectively. The plot of $\Gamma_x$, which measures the perturbation vorticity amplitudes, illustrates the evolution of these flows which generally consists of three phases (Laporte and Corjon, 2000): transient, linear, and nonlinear. During the transient phase ($t^* < 1$), the perturbation field decreases. The vortices adapt to the presence of each other in an essentially two-dimensional process. Due to the induced velocity, they propagate downwards and develop an elliptic shape due to the mutually induced strain. The effects of stratification are not yet three-dimensional and the behavior of the unstratified and stratified flows are similar. The linear phase is marked by the development of the short wave instability which is indicated by a corresponding growth in $\Gamma_x$ although $\Gamma_x \ll \Gamma_y$. The onset of the linear phase is earlier for the stratified flows and the growth rate of $\Gamma_x$ increases with level of stratification (lower $Fr$). In the nonlinear phase, the perturbation amplitudes become significant. $\Gamma_x$ reaches a peak and then decreases.

The time development of the circulation, $\Gamma$ (axial average for one vortex), is shown in Fig. 2. In the unstratified flow ($Fr = \infty$), $\Gamma$ exhibits a moderate decrease in the linear phase and a more significant decay in the nonlinear phase. In the stratified flows, $\Gamma$ is seen to decrease significantly through both the linear and nonlinear phases. This is due to the generation of baroclinic torque. As the vortex pair descends through the stably stratified fluid, it transports lighter fluid into a region of heavier fluid (Fig. 4a). Strong horizontal density gradients are thereby established which generate axial vorticity of opposite sign through baroclinic torque (Fig. 4b). This vorticity is included in $\Gamma$ and results in the reduced values. Figure 5 shows a conditional average circulation $\langle\Gamma\rangle_{\omega_{y+}}$ (conditioned on $\omega_y > 0$) which effectively excludes the baroclinic vorticity and provides a measure of the circulation of the primary vortex. In the stratified flows, $\langle\Gamma\rangle_{\omega_{y+}}$ shows a moderate reduction during the linear phase and an enhanced decay during the nonlinear phase. The rate of decay increases with level of stratification. At late times, this simple conditional averaging is no longer meaningful due to the complexity of the flow.

Figures 6 and 7 show the development of vortex structures in the unstratified ($Fr = \infty$) and stratified ($Fr = 2$) flows, respectively, during the linear and nonlinear phases. The structures are visualized by isosurfaces of the second invariant of the velocity gradient tensor, $II = (\omega^2/2 - \mathsf{S}^2)/2$ (where $\omega$ is vorticity, $\mathsf{S}$ is the strain rate tensor). The linear and nonlinear phases will each be discussed in more detail in the following sections.

### Linear Phase

In the unstratified flow, following the transition phase a dominant wavelength is selected and amplified deforming the vortices in a sinusoidal manner (Fig. 6, $t^* = 10.5$). As discussed in Leweke and Williamson (1998), the short wave instability is an elliptic instability which evolves in the vortex pair in a coupled "cooperative" manner. Close examination of the vortices reveals the distinct geometry associated with this instability. The deformation is in phase when viewed from the top ($x - y$ plane) and out-of-phase when viewed from the side ($y - z$ plane); the core displacements are of an antisymmetric mode. In the $x - z$ plane (front view), the deformation of each vortex is oriented in a plane approximately $30° - 40°$ from the horizontal. This direction corresponds to the direction of the principal extensional strain (Leweke and Williamson, 1998).

In the stratified flow, the instability is observed earlier in time (Fig. 7, $t^* = 5.25$), consistent with $\Gamma_x$ in Fig. 3. The basic geometric features of the elliptic instability are retained although the angle of the deformation plane from the horizonal is much greater (approximately $50° - 60°$ for $Fr = 2$). In addition, the separation distance, $b$, between the two vortices decreases in time. This is due to the secondary flow associated with the opposite sign baroclinic torque which advects the primary vortices towards one another. Figure 8 shows $b/b_o$ as a function of time for various $Fr$. With increasing stratifcation, $b$ is reduced more rapidly. The enhanced strain that occurs when the vortices are closer together causes the earlier onset of the instability.

In order to carry out a quantitative assessment of the linear phase, the wavelength, $\lambda_k$, of the most amplified mode and the corresponding growth rate, $\sigma$, are determined. The spectral energy, $E(k,t) = \overline{\widehat{v}^2}(k,t)$, is obtained by performing a one-dimensional Fourier transform in the axial ($y$) direction of the velocity, $\widehat{v} = \widehat{v}(x,k,z,t)$, and then evaluating the average in the transverse ($x-z$) plane, $\overline{\widehat{v}^2}(k,t)$. The most amplified mode, $k = k_{max}$, can be determined from $E(k,t)$. Since the base flow is two-dimensional in the $x - z$ plane, $E(k \geq 1, t)$ indicates the perturbation energy. Figures 9 and 10 shows $E(k,t^*)$ for $Fr = \infty$ and $Fr = 2$, respectively . At $t^* = 0$, the spectrum is flat corresponding to the initial random perturbation field. Beyond the transition phase, the perturbation energy increases at the low wavenumbers. In the unstratified flow (Fig. 9), a dominant wave number, $k_{max} = 6$, is identified which corresponds to the most amplified wavelength, $\lambda/b_o = 1.0$. This compares reasonably well with the reported wavelength of $\lambda/b_o = 0.77$ in Leweke and Williamson (1998). Figure 11 shows the time development of $E(k_{max},t)$. The growth rate, $\sigma$, of the most amplified mode energy is obtained from $\sigma = 1/2(d\,lnE_{k_{max}}/dt)$. For $Fr = \infty$, $\sigma^* = \sigma/(\Gamma/2\pi{b_o}^2) = 0.83$. The growth rate measured in the experiments is $\sigma^* = 0.94 \pm 0.12$. Overall, results for the unstratified flow are in agreement with the experiments of Leweke and Williamson (1998).

Figure 11 suggests that the growth rate increases with increasing stratification. However, in the stratified flows, the perturbation energy also includes that associated with secondary flow arising from stratification effects (baroclinic torque). Thus, $\lambda/b_o$ and $\sigma^*$ are determined using an alternative method based on Fourier transforms of the vortex core displacements. Results show that $\lambda$ is the same as that in the unstratified flow ($\lambda/b_o = 1.0$), however a significant increase in $\sigma$ is exhibited. This is due to the enhanced induced

Table 1: Growth rate, $\sigma^*$, from core displacement.

| $Fr$ | 2 | 5 | $\infty$ |
|---|---|---|---|
| $\sigma^*$ | 1.9 | 1.3 | 0.72 |

strain in the vortices, resulting from the reduced vortex separation distance, which accelerates the instability. Table 1 lists computed $\sigma^*$ as a function of $Fr$ which shows that as the stratification increases, $\sigma^*$ increases.

### Nonlinear Phase

The early stage of the nonlinear phase for $Fr = \infty$ is marked by the formation of "knobs" which appear at the peaks of the sinusoidal deformation (Fig. 6, $t^* = 13.5$). Vorticity concentrates within the knobs as indicated in the subsequent figure ($t^* = 15.0$). During this time, the spectrum exhibits the development of harmonics of the primary instability (Fig. 9, $12 \leq t^* \leq 15$). At times $t^* = 15.0$ to 16.5 (Fig. 6), secondary transverse vortex structures are observed to develop on the upstream side of the vortex pair. The formation of these structures are explained by considering the distinct geometry of the primary instability which brings the primary vortices closer together at the leading edge of the vortex pair (see $t^* = 12.0$ in Fig. 6). As discussed in Leweke and Williamson (1998), the phase relationship of the deformation is such that inner and outer layers of a vortex are displaced in opposite directions. At the leading edge, the outer layers of one vortex is in proximity to the inner core of the other which leads to the extraction of fluid from one vortex into the other (Fig. 12a). As indicated in Fig. 2, this process results in a more rapid reduction in $\Gamma$. The azimuthal vorticity occuring in the outer layers (see Leweke and Williamson, Fig. 12), which includes the transverse component, $\omega_x$, is amplified through vortex stretching by the extensional strain at the leading stagnation point. Subsequently, $\omega_x$ becomes the dominant component of vorticity and the associated structure extends over the leading edge of the vortex pair oval (Fig. 6, $t^* = 16.5$). An array of transverse counter-rotating vortex pairs results, two pairs for every wavelength of the primary instability. The corresponding spectrum (not shown) exhibits the primary mode and first harmonic but the higher wavenumber modes are no longer distinct. For times, $t^* > 15$, the primary instability becomes saturated and the corresponding growth rate is reduced to zero. It is interesting to note that at $t^* = 18.0$, the corresponding energy spectrum (Fig. 9) is quite broad with no preferred mode although coherent structures remain in the flow (Fig. 6). Evidently, there is sufficiently complex small-scale structure and effective energy transfer across all modes. Laporte and Corjon (2000) suggest that transition to turbulence is indicated when all modes have reached the same order of magnitude and all growth rates are zero or less. Late time spectra ($t^* > 18.0$) for the present results do indicate growth rates of zero or less for all modes.

In the stratified flow, knob structures also initially form (Fig. 7, $t^* = 6.0$). The corresponding energy spectrum (Fig. 10) shows the development of the harmonics. The extraction of outer layer fluid from one vortex into the other at the leading edge of the vortex pair also occurs (Fig. 12b). However, the transverse structures observed in the $Fr = \infty$ are no longer significant (Fig. 7). This is due to the deceleration of the vortex pair descent caused by baroclinic torque which results in a reduced extensional strain at the leading edge. Consequently, amplification of $\omega_x$ at the leading stagnation point is not as significant. Alternatively, pairs of counter-rotating vertical structures develop, between and above the primary vortices, with one pair for every wavelength of the primary instability (Fig. 7, $t^* = 6.75$). Such vortex structures are also observed in the simulation results of Delisi and Robbins (2000) and Holzäpfel et al. (2001). An enhanced extensional strain in between the vortices, caused by the reduced separation distance, amplifies the azimuthal vorticity ($\omega_z$) existing between the primary vortices which leads to the formation of the vertical structures. By $t^* = 7.5$, $\omega_z$ is the dominant component of vorticity in the flow. The corresponding spectrum (Fig. 10, $t^* = 6.75$) shows the development of the first harmonic. Beyond this time, the primary mode saturates and the spectrum broadens at the high wavenumbers. The peaks associated with the primary mode and first harmonic are retained due to the generated baroclinic torque which persists downstream of the vortex pair (Fig. 12). Although the spatial structure at this late stage differs signficantly from the unstratified flow, the behavior of the energy spectrum is similar. In regards to the breakdown of the flow, the counter-rotating vertical structures enable an *additional* mechanism of fluid exchange in the transverse direction. This is observed in Fig. 12b which shows axial vorticity ($\omega_y > 0$) from the left vortex transported to the right side both at the leading edge (extraction by right vortex) and above the vortex oval (by secondary vertical structure). In addition, there is detrainment of the primary vortices by the secondary baroclinic vortex structures on the downstream side. These additional mechanisms of vortex breakdown result in a more rapid decay of the the vortex pair in the stratified flow (Fig. 5).

### Summary and Conclusions

The effect of stably stratification on the development of the short-wave instability and subsequent decay of a counter-rotating vortex pair is investigated using DNS. A range of Froude numbers, $2 \leq Fr \leq \infty$ is considered. In the linear phase, the short-wave instability develops with the same wavelength and geometric features in both unstratified and stratified flows. However, an earlier onset and a higher growth rate are exhibited with increasing levels of stratification, This is due to the enhanced strain that occurs when the vortices move closer together as a result of the generated baroclinic torque. In the early stages of the nonlinear phase, the evolution of both unstratified and stratified flows are controlled by the distinct geometry of the short-wave instability. The phase relationship of the initial deformation results in periodic extraction of outer layer fluid from one vortex into the other at the leading edge of the vortex pair. This initiates the vortex breakdown process in the unstratified flow. The azimuthal vorticity in the outer layers of the primary vortices are amplified due to the extensional strain at the leading stagnation point and transverse secondary vortex structures are formed. In the stratified flows, effects of baroclinic torque inhibit the formation of the transverse structures. Alternatively, amplification of the azimuthal vorticity in between the primary vortices leads to the formation of vertical vortex structures. This establishes an additional mechanism of exchange of fluid in the transverse direction. Detrainment of the primary vortices by the generated baroclinic torque also contributes to the breakdown of the vortices. These additional mechanisms lead to a more rapid decay of the the vortex pair in the stratified flows.

References


[1] Crow, S. C. (1970). Stability theory for a pair of trailing vortices. *AIAA J.*, 8:2172–2179.

[2] Delisi, D. P. and Robbins, R. E. (2000). Short-scale instabilities in trailing wake vortices in a stratified fluid. *AIAA J.*, 38:1916–1923.

[3] Garten, J. F., Werne, J., Fritts, D. C., Arendt, S. (2001). Direct numerical simulations of the Crow instability and subsequent vortex reconnection in a stratified fluid. *J. Fluid Mech.*, 426:1–45.

[4] Gerz, T., Schumann, U., and Elghobashi, S. (1989). Direct simulation of stably stratified homogeneous turbulent shear flows. *J. Fluid Mech.*, 200:563–594.

[5] Holzäpfel, F., Gerz, T., Baumann, R. (2001). The turbulent decay of trailing vortex pairs in stably stratified environments. *Aerosp. Sci. Technol.*, 5:95–108.

[6] Laporte, F. and Corjon, A. (2000). Direct numerical simulations of the elliptic instability of a vortex pair. *Phys. Fluids*, 12:1016–1031.

[7] Leweke, T. and Williamson, C. H. K. (1998). Cooperative elliptic instability of a vortex pair. *J. Fluid Mech.*, 360:85–119.

[8] Sarpkaya, T. and Suthon, P. (1991). Interaction of a vortex couple with a free surface. *Exp. Fluids*, 11:205.

[9] Switzer, G. and Proctor, F. (2000). Numerical study of wake vortex behavior in turbulent domains with ambient stratification. *38th Aerospace Sciences Meeting & Exhibit*, AIAA 2000-0755, Reno, NV.

[10] Thomas, P. J. and Auerbach, D. (1994). The observation of the simultaneous development of a long and short-wave instability mode on a vortex pair. *J. Fluid Mech.*, 256:289.


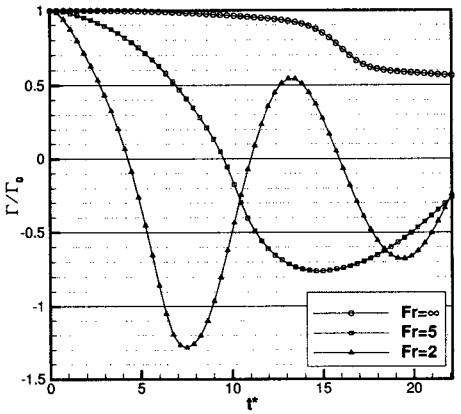


Figure 2: Time development of vortex circulation, $\Gamma$.

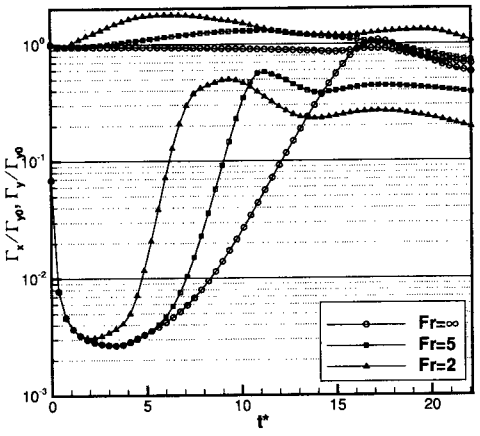


Figure 3: Evolution of normalized average axial and transverse vorticity magnitudes, $\Gamma_y/\Gamma_{y,0}$ (upper set of curves) and $\Gamma_x/\Gamma_{y,0}$ (lower set of curves), respectively.

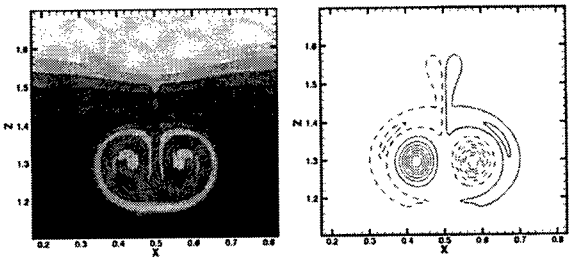

a. $\rho$ b. $\omega_y$

Figure 4: Contours in $x-z$ plane for $Fr = 2$ at $t^* = 2.25$ of a. density, $\rho$ and b. axial vorticity, $\omega_y$ (solid: $\omega_y > 0$, dash: $\omega_y < 0$).

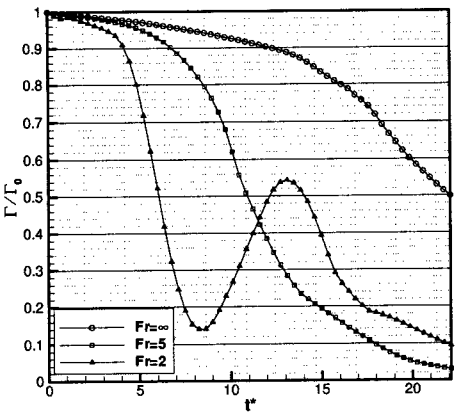


Figure 5: Time development of conditional vortex circulation, $\langle\Gamma\rangle_{\omega_{y+}}$ (conditioned by $\omega_y > 0$).

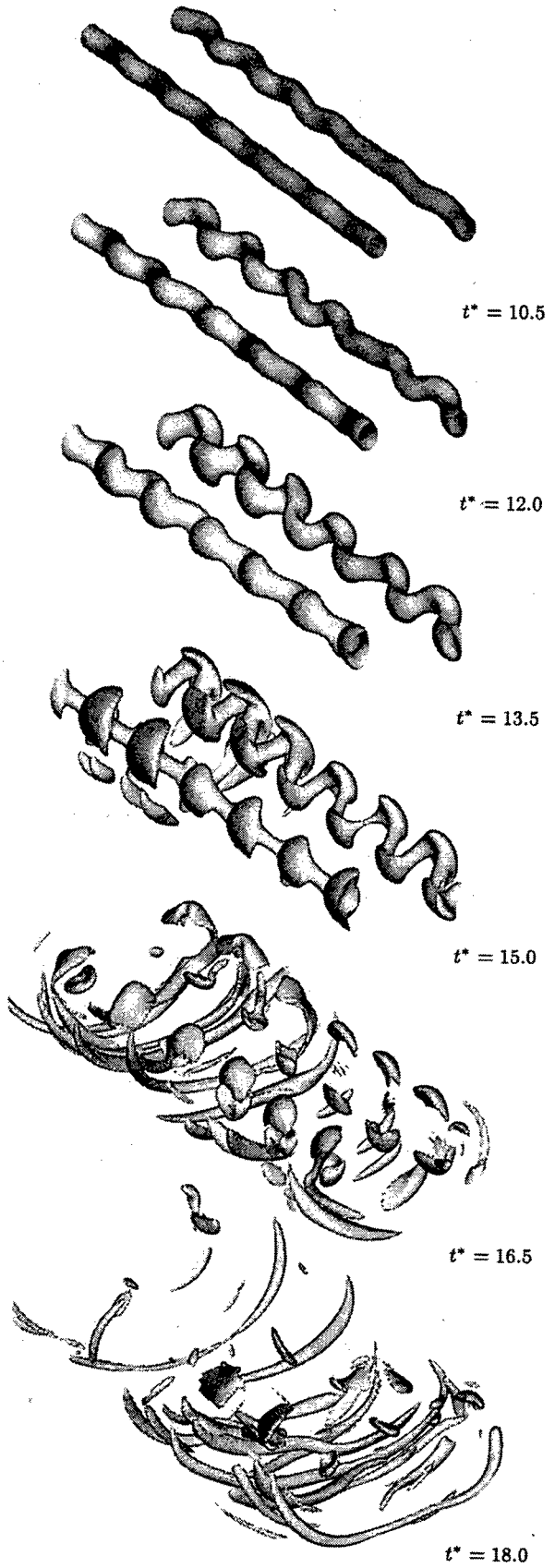


Figure 6: Three-dimensional visualizations of isosurfaces of second invariant of velocity gradient tensor, $II$ for $Fr = \infty$ at times $t^* = 10.5, 12.0, 13.5, 15.0, 16.5, 18.0$.

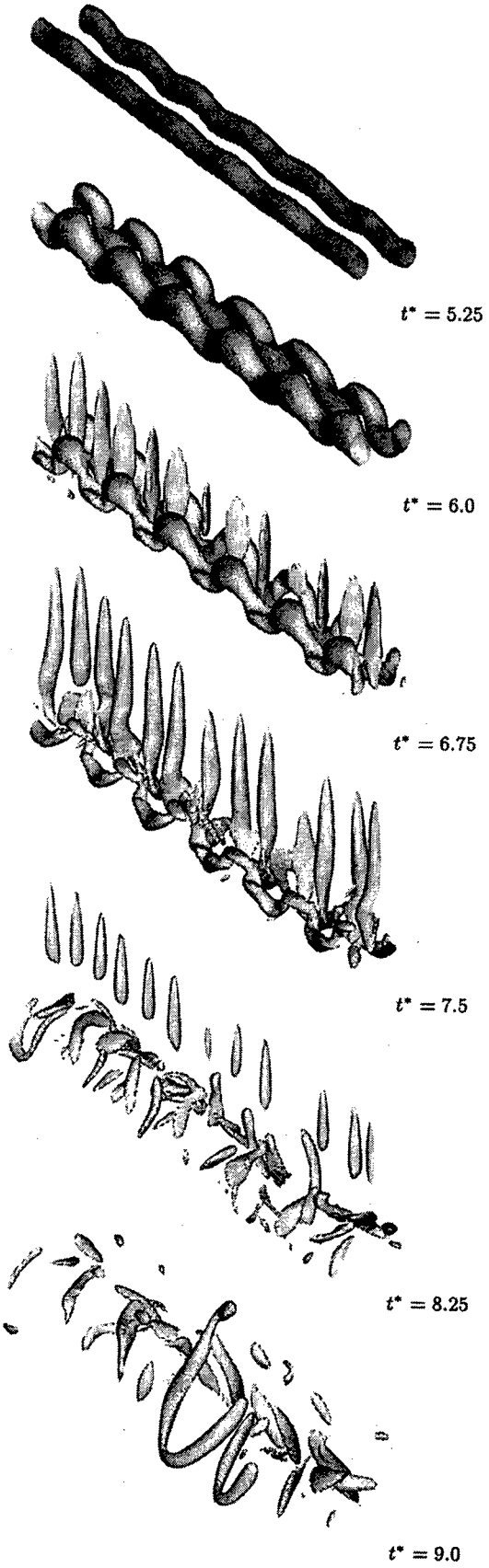


Figure 7: Three-dimensional visualizations of isosurfaces of second invariant of velocity gradient tensor, $II$ for $Fr = 2$ at times $t^* = 5.25, 6.0, 6.75, 7.5, 8.25, 9.0$.

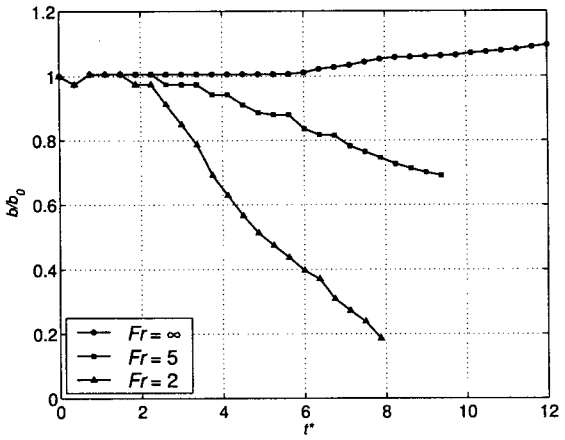


Figure 8: Vortex separation distance as a function of time.

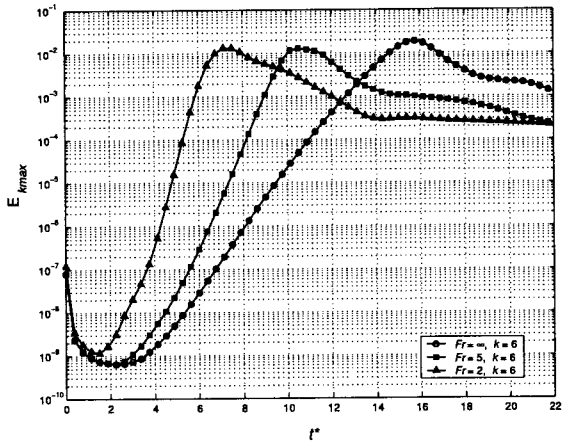


Figure 11: Evolution of perturbation energy of most amplified mode, $k = k_{max}$.

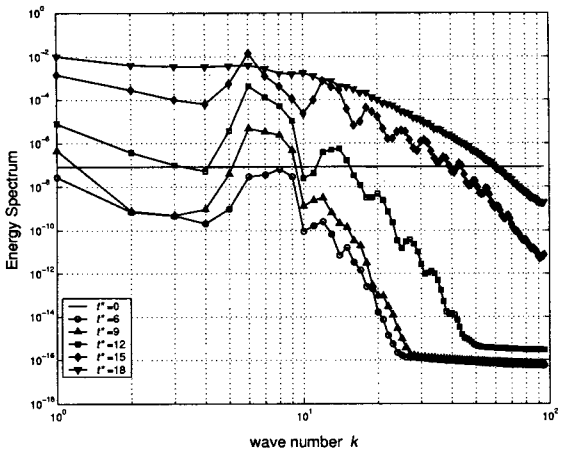


Figure 9: Kinetic energy spectrum for $Fr = \infty$.

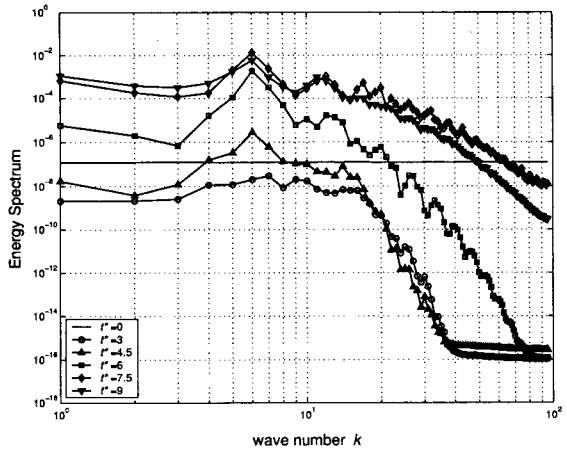


Figure 10: Kinetic energy spectrum for $Fr = 2$.

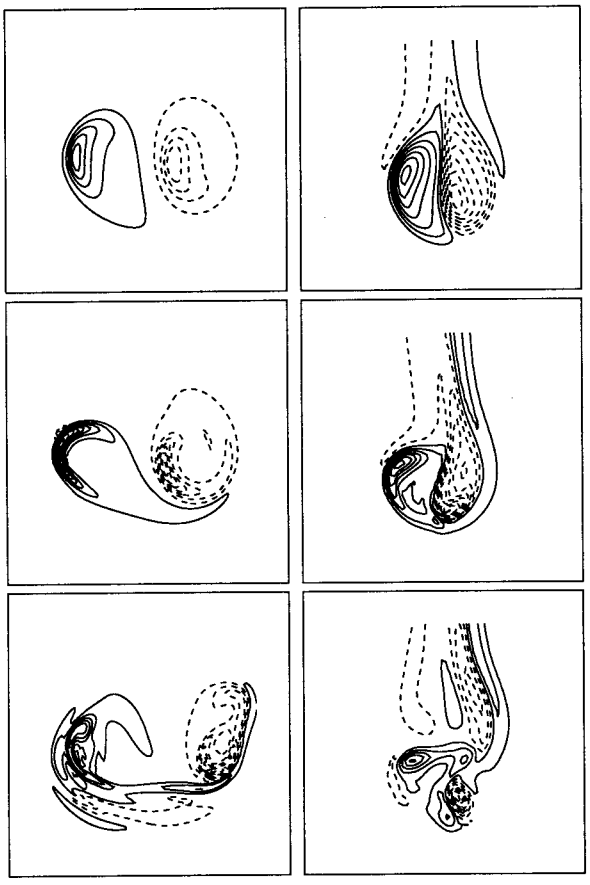

a. $Fr = \infty$ b. $Fr = 2$

Figure 12: Contours of axial vorticity, $\omega_y$, in $x - z$ plane for a. $Fr = \infty$ at $t^* = 13.5, 15.0, 16.5$ and b. $Fr = 2$ at $t^* = 6.0, 6.75, 7.5$ (solid: $\omega_y > 0$, dash: $\omega_y < 0$).